

***In vitro* cytocompatibility of one-dimensional and two-dimensional nanostructure-reinforced biodegradable polymeric nanocomposites**

Behzad Farshid,^{1,2} Gaurav Lalwani,¹ Balaji Sitharaman¹

¹Department of Biomedical Engineering, Stony Brook University, Stony Brook, New York 11794

²Department of Materials Science and Engineering, Stony Brook University, Stony Brook, New York 11794

Received 7 August 2014; revised 4 October 2014; accepted 22 October 2014

Published online 19 November 2014 in Wiley Online Library (wileyonlinelibrary.com). DOI: 10.1002/jbm.a.35363

Abstract: This study investigates the *in vitro* cytocompatibility of one-dimensional and two-dimensional (1D and 2D) carbon and inorganic nanomaterial reinforced polymeric nanocomposites fabricated using biodegradable polymer poly (propylene fumarate), crosslinking agent *N*-vinyl pyrrolidone (NVP) and following nanomaterials: single and multiwalled carbon nanotubes, single and multiwalled graphene oxide nanoribbons, graphene oxide nanoplatelets, molybdenum disulfide nanoplatelets, or tungsten disulfide nanotubes dispersed between 0.02 and 0.2 wt% concentrations in the polymer. The extraction media of unreacted components, crosslinked nanocomposites and their degradation products were examined for effects on viability and attachment using two cell lines: NIH3T3 fibroblasts and MC3T3 preosteoblasts. The extraction media of unreacted PPF/NVP elicited acute dose-dependent cytotoxicity attributed to leaching of unreacted components into cell culture media. However, extraction media of crosslinked nanocomposites showed no dose dependent adverse effects. Further, all crosslinked

nanocomposites showed high viability (78–100%), high cellular attachment (40–55%), and spreading that was confirmed by confocal and scanning electron microscopy. Degradation products of nanocomposites showed a mild dose-dependent cytotoxicity possibly due to acidic degradation components of PPF. In general, compared to PPF control, none of the nanocomposites showed significant differences in cellular response to unreacted components, crosslinked nanocomposites and their degradation products. Initial minor cytotoxic response and lower cell attachment numbers were observed only for a few nanocomposite groups; these effects were absent at later time points for all PPF nanocomposites. The favorable cytocompatibility results for all the nanocomposites opens avenues for *in vivo* safety and efficacy studies for bone tissue engineering applications. © 2014 Wiley Periodicals, Inc. *J Biomed Mater Res Part A*: 103A: 2309–2321, 2015.

Key Words: graphene, inorganic nanomaterials, cytotoxicity, nanocomposites, tissue engineering, biodegradable polymers

How to cite this article: Farshid B, Lalwani G, Sitharaman B. 2015. *In vitro* cytocompatibility of one-dimensional and two-dimensional nanostructure-reinforced biodegradable polymeric nanocomposites. *J Biomed Mater Res Part A* 2015;103A:2309–2321.

INTRODUCTION

Biodegradable polymers such as poly(lactic-co-glycolic acid) (PLGA),¹ poly(propylene fumarate) (PPF),² and nonbiodegradable polymers such as polyurethane (PU)³ have been used to develop coatings for metallic implants¹ and nonporous prosthetic polymeric components such as compact rods⁴ and interference screws.⁵ The biodegradable polymers have also been broadly used to fabricate porous scaffolds to treat bone loss due to fractures, traumatic musculoskeletal injuries, congenital abnormalities, or other bone defects.^{6–10} For applications involving load bearing implants, these polymers lack adequate mechanical properties.¹¹ Studies show that incorporation of carbon and inorganic nanomaterials such as fullerenes,¹² carbon nanotubes (CNTs)¹³ and alu-

moxane nanomaterials¹⁴ as reinforcing agents into these polymers significantly improves their mechanical properties.¹⁵

Recently, we systematically investigated the efficacy of one-dimensional and two-dimensional (1D and 2D) organic and inorganic nanomaterials as reinforcing agents to improve the mechanical properties (compressive and flexural modulus, and yield strength) of the polymer PPF. Single and multiwalled CNTs (SWCNTs and MWCNTs), single and multiwalled graphene oxide nanoribbons (SWGONRs, MWGONRs), graphene oxide nanoplatelets (GONPs), molybdenum disulfide nanoplatelets (MSNPs), or tungsten disulfide nanotubes (WSNTs) were dispersed into PPF at various loading concentrations (0.01–0.2 wt %). These nanomaterial-reinforced PPF

Additional Supporting Information may be found in the online version of this article.

Correspondence to: Balaji Sitharaman, Ph.D.; e-mail: balaji.sitharaman@stonybrook.edu

Contract grant sponsor: National Institute of Health; contract grant number: 1DP2OD007394-01

Contract grant sponsor: U.S. Department of Energy [DOE; Center for Functional Nanomaterials, Brookhaven National Laboratory (Upton, New York)]; contract grant number: DE-AC02-98CH10886

nanocomposites exhibited mechanical properties (e.g., 1–1.6 GPa compressive modulus) that was similar to cancellous bone (0.3–10 GPa compressive modulus).^{16,17}

Along with the efficacy studies, *in vitro* cytotoxicity and *in vivo* biocompatibility of nanomaterials-incorporated polymers needs to be thoroughly investigated. *In vitro* studies are typically the first step to screen various nanomaterial and nanocomposite formulations prior to significantly elaborate and costly *in vivo* animal experiments.¹² Various *in vitro* studies have investigated the cytotoxicity of SWCNTs,¹⁸ MWCNTs,¹⁹ GONPs,^{20,21} GONRs,^{22,23} MSNPs,²⁴ and WSNTs.²⁵ A few studies have investigated the *in vitro* cytotoxicity and *in vivo* biocompatibility of nonporous PPF nanocomposites^{26,27} and porous PPF scaffolds containing SWCNTs^{28,29} and alumoxane nanomaterials.^{14,30,31} The *in vitro* cytotoxicity of other carbon nanomaterials-reinforced PPF nanocomposites (MWCNTs, SWGONRs, MWGONRs, and GONPs) and inorganic nanomaterials-reinforced PPF nanocomposites (WSNTs and MSNPs) has not been reported. Cytocompatibility of some of these nanomaterials incorporated into other polymer nanocomposites such as PLGA (nonporous CNT/PLGA³² and porous GONP/PLGA³³), and PU (porous GONP/PU scaffolds³⁴) has been investigated.

In this study, we have systematically examined the cytocompatibility of various 1D and 2D carbon (SWCNTs, MWCNTs, SWGONRs, MWGONRs, and GONPs) and inorganic (WSNTs and MSNPs) nanomaterials-reinforced PPF nanocomposites using NIH3T3 fibroblasts and MC3T3 preosteoblasts. The comprehensive cytocompatibility assessment included assays to characterize the cytotoxicity of unreacted components, crosslinked nanocomposites, and their degradation products. Additionally, cell attachment and proliferation studies were performed on the crosslinked nanocomposites.

MATERIALS AND METHODS

Synthesis of nanomaterials and nanocomposites

Materials. Diethyl fumarate, hydroquinone, *N*-vinyl pyrrolidone (NVP), potassium permanganate, zinc chloride, benzoyl peroxide (BP), graphite, molybdenum trioxide, sulfur, and MWCNTs were purchased from Sigma Aldrich (St. Louis, MO). Other analytical grade materials: hydrogen peroxide, ethyl ether, sodium sulfate, methylene chloride, isopropanol, ethanol, chloroform, hydrochloric acid, phosphoric acid, sulfuric acid, and calcium hydroxide were purchased from Fisher Scientific (Pittsburgh, PA). Propylene glycol was obtained from Acros Organics (Pittsburgh, PA). SWCNTs were purchased from Cheap Tubes Incorporated (Battletown, VT), and WSNTs were donated by Nanomaterials Limited (Yavne, Israel).

Polymer synthesis. PPF was synthesized using a well-established two-step reaction of propylene glycol and diethyl fumarate.³⁵ It was characterized using proton nuclear magnetic resonance spectroscopy (¹H-NMR, 300Hz, Oxford instruments, Oxford, UK) and high performance liquid chromatography (Accela 600 HPLC, Thermo Scientific, Waltham, MA) as described previously.^{16,17}

Nanomaterial synthesis. SWGONRs and MWGONRs were synthesized by an oxidative unzipping method developed by Kosynkin et al. using SWCNTs and MWCNTs as starting material.³⁶ GONPs were synthesized utilizing the modified Hummer's method (the modified technique allows synthesis of macroscopic quantities of GONPs through additional dispersing and filtration steps compared to the conventional Hummer's method³⁷). MSNPs were synthesized using well established chemical method using molybdenum trioxide and sulfur as starting materials.³⁸

Nanocomposite fabrication

PPF nanocomposites were fabricated as reported previously.^{16,17} The loading concentration of each nanomaterial was the concentration that yielded the maximum compressive modulus in our previous study.^{16,17} Briefly, PPF and NVP were mixed in chloroform followed by addition of 0.02 wt % SWCNTs, 0.1 wt % of MWCNTs, SWGONRs, MWGONRs, GONPs, and 0.2 wt % of WSNTs and MSNPs. The PPF, NVP, and nanomaterial blends were subjected to bath sonication for 30 min (FS30H bath sonicator, Fisher Scientific, Madison, CT) followed by probe sonication for 2 min (2 sec "on" and 1 sec "off" cycle; LPX-750 sonicator, Cole Parmer, Vernon Hills, IL). Chloroform was removed using a rotavapor (R-215, Büchi, New Castle, DE), and thermal crosslinking of nanocomposite was initiated by addition of 1 wt % BP radical initiator. The crosslinking of nanocomposites was completed overnight at 60°C inside a custom made Teflon® mold (McMaster-carr, Princeton, NJ). Cylindrical crosslinked specimens with diameter of 6.5 mm and height of 14 mm were cut into disks of 1 mm thickness by a low-speed diamond saw (Model 650, South Bay Technology, Redondo Beach, CA) and used for *in vitro* studies.

Characterization of nanomaterials and nanocomposites

Raman spectroscopy. A WITec spectrometer (α-300R, Chicago, IL) recorded the Raman spectra in the wavenumber range of 100–2900 cm⁻¹ using an excitation wavelength of 532 nm. For sample preparation, 1 mg of nanomaterials was dispersed in a (50:50) mixture of ethanol-distilled water inside a 1.5 mL microcentrifuge tube (Eppendorf AG, Hauppauge, NY) and subjected to bath sonication for 30 min and then probe sonication for 2 min (2 sec "on" and 1 sec "off" cycle). Next, the microcentrifuge tube underwent 5 min of centrifugation at 5000 rpm. Twenty microlitres of its content was drop casted on freshly cleaved silicon wafers (Ted Pella, Redding, CA), air-dried, and used for Raman spectroscopy.

Transmission electron microscopy. Transmission electron microscopy (TEM) samples were prepared using 10 µL of nanomaterial dispersions prepared for Raman analysis. The dispersions were drop casted on TEM grids (300 mesh sizes, lacey carbon grids, Ted Pella, Redding, CA) and air dried overnight. TEM was performed using a TECNAI BioTwin G² transmission electron microscope (FEI Technologies, Hillsboro, OR) at an accelerating voltage of 80 kV.

Scanning electron microscopy. Scanning electron microscopy (SEM) imaging was performed using a JEOL 7600F high resolution SEM microscope (JEOL, Peabody, MA) at the Center for Functional Nanomaterials, Brookhaven National Laboratory, NY. A double-sided carbon adhesive tape (Pelco®, Ted Pella, Redding, CA) was used to fix nanocomposite discs onto the SEM sample holders. These specimens were sputter-coated with 3 nm of gold to prevent charge accumulation. Secondary electron imaging (SEI) detector was used to image samples at an accelerating voltage of 5 kV.

In Vitro studies

Cell culture. NIH3T3 fibroblasts (passages 24–27) and MC3T3 preosteoblasts (passages 10–14) were used for cytocompatibility studies. Dulbecco's modified eagle medium (DMEM, Gibco Life Technologies, Grand Island, NY) and minimum essential medium alpha (MEM- α , Gibco Life Technologies) media, supplemented with 10 vol % fetal bovine serum (FBS, Gibco Life Technologies) and 1 vol % antibiotics (penicillin-streptomycin, Gibco Life Technologies, Grand Island, NY) were used to culture NIH3T3 and MC3T3 cells, respectively. Blank media refers to unaltered DMEM and MEM- α media containing supplements. Cells were lifted using trypsin-EDTA (1X, Gibco Life Technologies, Grand Island, NY) and seeded in a 96-well plate (BD Falcon, Franklin Lakes, NJ) at cell density of 5000 cells/well (15,625 cells/cm²). After incubation for 24 h, wells were washed with Dulbecco's phosphate buffered saline solution (DPBS, Gibco Life Technologies, Grand Island, NY) and incubated with cell culture media called experimental media. This media was prepared by a direct extraction method according to ISO 10993-5.⁴³ Treatment duration was 24 h and the treated cells were kept in humidified (95% air and 5% carbon dioxide) incubator operating at 37°C temperature.

Presto blue assay. Cell viability was assessed using presto blue assay according to manufacturer's protocol. NIH3T3 and MC3T3 cells were seeded in a 96-well plate at a density of 5,000 cells/well (15,625 cells/cm²). After 24 h treatment, 10- μ L presto blue was added to each well. After 2 h of incubation, fluorescence readings were recorded using a Cytoflour4000 plate reader (McKinley Scientific, Sparta Township, NJ) at excitation and emission wavelengths of 530 and 590 nm, respectively. Wells with 5000 viable cells (no treatment) served as a positive (live) control. Wells containing cells treated with PPF experimental media served as a baseline control and wells with blank media (without cells) served as a negative control. Sample size was $n = 6$ for this assay. Fraction of viable cells was determined using equation:

$$\text{Fraction of live cells} = (F_S/F_L)$$

where F_S is the fluorescence of each well after background subtraction, and F_L is the average fluorescence of positive (live) control after background subtraction.

Lactate dehydrogenase assay. Membrane integrity of cells was characterized using lactate dehydrogenase (LDH) Assay

(TOX-7, Sigma Aldrich, St. Louis, MO) according to manufacturer's protocol. NIH3T3 and MC3T3 cells were seeded in a 96-well plate at a density of 5,000 cells/well (15,625 cells/cm²) and incubated for 24 h. After incubation, the media was replaced with the experimental media. After 24 h treatment, the culture plates were centrifuged at a speed of 1200 rpm to remove cellular debris. Fifty microlitres of the supernatant media was transferred to a fresh 96-well plate followed by addition of 100 μ L LDH assay reagent to each of the wells. After incubation for 40 min in dark, the absorbance was recorded at 490 nm using a Biotek EL800 plate reader (Winooski, VT). To the wells with 5000 viable cells, 10 μ L lysis solution was added for 15 min (TOX-7, Sigma Aldrich, St. Louis, MO) to lyse the cells, and these wells served as positive (dead) controls. Wells treated with experimental media of PPF polymer served as a baseline control. Wells containing blank media (without cells) served as a negative control. Sample size was $n = 6$ for this assay. Fraction of dead cells was calculated using following equation:

$$\text{Fraction of dead cells} = A_S/A_D$$

where A_S is the absorbance of each well after background subtraction, and A_D is the average absorbance of positive (dead) control after background subtraction.

Calcein-AM (LIVE) assay. Calcein-AM (calcein acetoxymethyl ester) was used to stain the adherent viable cells on the surface of nanocomposites after 1 and 5 days of incubation. Five microlitres of calcein-AM stock solution (40 mM concentration, Sigma Aldrich, St. Louis, MO) was added to 10 mL DBPS and then added to the crosslinked nanocomposite disks (100,000 cells/specimen or 3×10^5 cells/cm²). The disks were incubated at 37°C. After incubation for 30 min in dark, samples were washed with DPBS prior to confocal imaging. Fluorescence images were recorded using an excitation wavelength of 485 nm and an emission wavelength of 530 nm. 96-well plate (TCPS control) containing 100,000 (3.12×10^5 cells/cm²) seeded cells served as a positive control whereas blank wells containing media served as a negative control. Sample size was $n = 3$ for calcein-AM staining.

In vitro studies to examine the effects of noncrosslinked macromers. A blend of PPF-NVP (50:50) was sterilized for 3 h under ultraviolet light (UV). Next, cell culture media was added to the blend and incubated for 24 h at 37°C (1 ml media per cm² contact area). The supernatant of this media was used for studies. As-prepared supernatant (labeled 1X experimental media) and its 10X and 100X dilutions (called 10X and 100X experimental media, respectively) were used to treat the cells. Viability of the cells was examined by presto blue and LDH assays after 24 h of incubation with 1X, 10X, or 100X experimental media. Sample size was $n = 6$ for each experimental group.

In vitro studies to examine the effects of crosslinked nanocomposites. Nanocomposite disks of 6.5 mm diameter and 1 mm thickness were sterilized under UV for 3 h and

incubated with cell culture media (1 mL media per cm² contact area). The supernatant media was then extracted and used for studies. As-prepared supernatant (labeled 1X experimental media) and its 10X and 100X dilutions (called 10X and 100X experimental media, respectively) were used to treat the cells. Cells were cultured inside a 96-well plate and incubated at 37°C for 24 h. Next, 1X, 10X, or 100X experimental media were added to these wells. Viability of the cells was analyzed after 24 h incubation with experimental media using presto blue and LDH assays. Sample size was $n = 6$ for each experimental group.

In vitro studies to examine the effects of degradation products from nanocomposites. Nanocomposite specimens underwent an expedited hydrolytic degradation process. 2.5 g of each nanocomposite was crushed and degraded for 14 days inside sealed 25-mL glass vials containing 0.25 *N* Ca(OH)₂ solution, kept on a shaker table at 100 rpm. The pH of the solution containing degradation product was adjusted to 7.4 using H₃PO₄, and then vacuum filtered using Whatman® filter paper (No. 40, Fisher Scientific, Pittsburg, PA). Degradation products do not contain ingredients and supplements found in regular cell culture media such as D-glucose, L-glutamine and FBS, therefore, the filtered solutions were diluted with cell culture media at 1:1 ratio to provide the necessary components. This 2X experimental media was further diluted to 10X and 100X folds using blank cell culture media to prepare 10X and 100X experimental media. Viability of the cells was assessed, after 24 h of incubation with the 2X, 10X, or 100X experimental media, by presto blue and LDH assays. PPF polymer served as a baseline control. Sample size was $n = 6$ for each experimental group. Osmolarity of unaltered DMEM, MEM- α and DPBS media after degradation was measured (sample size $n = 3$) using a 3D3 osmometer (Advanced Instruments, Norwood, MA).

In vitro studies to characterize the cell attachment and spreading on crosslinked nanocomposites. Crosslinked nanocomposites disks (6.5 mm diameter, 1 mm thickness) were sterilized for 3 hours using UV light and placed inside a six-well plate (BD Falcon, Franklin Lakes, NJ). Autoclaved stainless steel hollow weights were placed on top of each disk prior to cell culture to prevent floating of nanocomposite specimens and ensure proper cell seeding. Next, NIH3T3 and MC3T3 cells were seeded inside the rings at density of $\sim 400,000$ cells/specimen (1.2×10^6 cells/cm²). After incubation for 1 day, the nanocomposite specimens were washed and cells were detached and counted using a hemocytometer (Fisher Scientific, Pittsburg, PA). PPF polymer served as a baseline control and tissue culture polystyrene (TCPS) served as a positive control. To prepare positive control 400,000 cells were cultured inside a 96-well plate (surface area of each well = 28.27 mm², similar to nanocomposite disks). Sample size was $n = 3$ for each experimental group.

Confocal fluorescence microscopy was employed to visualize cell proliferation and spreading on the surface of nano-

TABLE I. The Experimental and Control Groups Used in this Study

Abbreviation	Name
PPF	poly(propylene fumarate)
SWCNTs	single walled carbon nanotubes
MWCNTs	multiwalled carbon nanotubes
SWGONRs	single walled graphene oxide nanoribbons
MWGONRs	multiwalled graphene oxide nanoribbons
GONPs	graphene oxide nanoplatelets
WSNTs	tungsten disulfide nanotubes
MSNPs	molybdenum disulfide nanoplatelets

composites. Cells were seeded at a density of 100,000 cells per specimen (3×10^5 cells/cm²), and incubated for 1 and 5 days. Subsequently, calcein-AM dye (Gibco Life Technologies, Grand Island, NY) was used to stain the attached cells. Disks were then placed inside a glass-bottom petridish (Mattek, Ashland, MA) and imaged using an LSM 510 (Carl Zeiss, Oberkochen, Germany) laser scanning confocal microscope with an emission wavelength of 515 nm. PPF polymer served as a baseline control, and wells of a 96-well TCPS plate initially seeded with 100,000 cells (3.12×10^5 cells/cm²) served as a positive control. Blank wells containing media served as a negative control. Sample size was $n = 3$ for each experimental group.

SEM was used to investigate cellular attachment and spreading on the nanocomposite disks. The samples for SEM were prepared as follows: Nanocomposite discs used for confocal microscopy were fixed using 2.5% glutaraldehyde solution, washed with ethanol (using 70, 80, 90, and 100% ethanol solutions) and dried in air and in vacuum for 24 h each. SEM was performed using a high-resolution JEOL 7600F HRSEM microscope (JEOL, Peabody, MA) at the Center for Functional Nanomaterials, Brookhaven National Laboratory, NY, at an accelerating voltage of 5 kV.

Statistical analysis

Statistical analysis was performed using a 95% confidence interval ($p < 0.05$). Single factor analysis of variance (one way ANOVA) followed by Tukey's *post hoc* test was performed to investigate significant differences between experimental groups. The data is presented as mean \pm standard deviation.

RESULTS

The experimental and control groups used in this study are listed in Table I.

Characterization of polymer and nanomaterials

The NMR spectra of PPF polymer is included in the supplementary information (Supporting Information Fig. 1S), and is similar to published spectra.³⁵ Figure 1(a–g) display representative TEM images of various nanomaterials. SWCNTs [Fig. 1(a)] and MWCNTs [Fig. 1(b)] were present as individual and bundled nanotubes. The diameter and length of SWCNTs were ~ 1 –2 nm and ~ 20 –30 μ m, respectively. The diameter and length for MWCNTs were ~ 20 –30 nm and ~ 200 μ m, respectively. TEM images of SWGONRs [Fig. 1(c)]

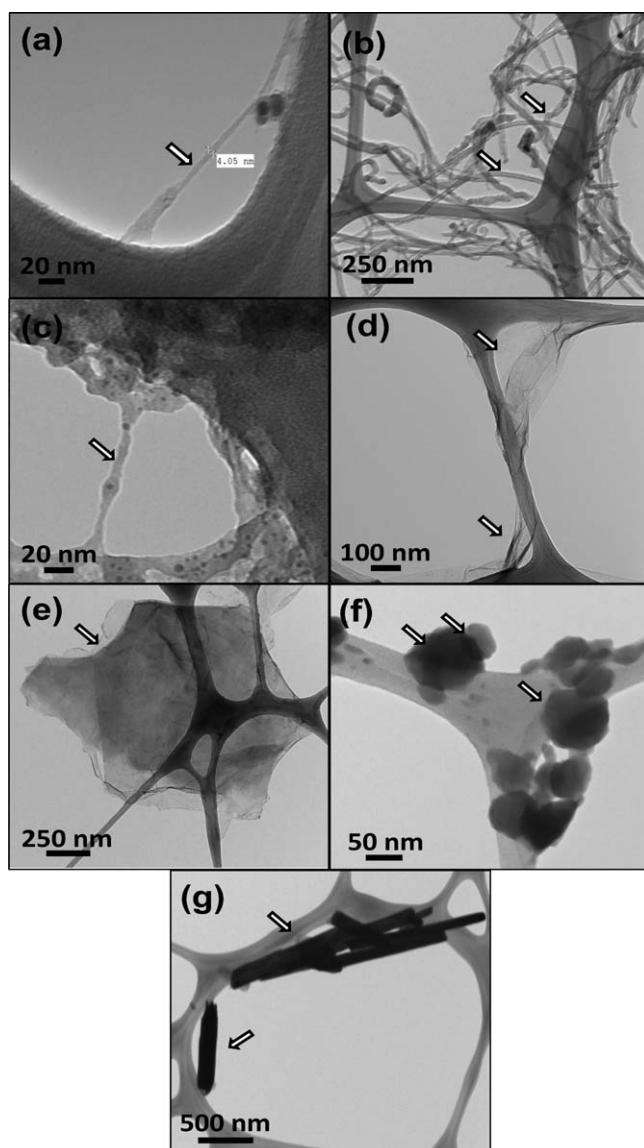


FIGURE 1. Representative TEM images of (a) single walled carbon nanotubes, (b) multiwalled carbon nanotubes, (c) single walled graphene oxide nanoribbons, (d) multiwalled graphene oxide nanoribbons, (e) graphene oxide nanoplatelets, (f) molybdenum disulfide nanoplatelets, and (g) tungsten disulfide nanotubes.

and MWGONRs [Fig. 1(d)] showed a smooth planar structure with few edge defects, and indicated the complete unzipping of SWCNTs and MWCNTs into nanoribbons (width of nanoribbons $\sim \pi \times$ diameter of nanotubes). The width and length of SWGONRs were ~ 4 nm and ~ 20 – 30 μm , respectively. The width and length for MWGONRs were ~ 20 – 30 nm and ~ 200 μm , respectively. GONPs [Fig. 1(e)] were disk shaped with ~ 200 – 1600 nm diameter and ~ 5 nm thickness. MSNPs [Fig. 1(f)] were hexagonal nanoplatelets with ~ 100 nm diameter and ~ 8 nm thickness. WSNTs [Fig. 1(g)] were tube-shaped with ~ 15 – 100 nm diameter and ~ 4 μm length.

Figure 2 shows Raman spectra of SWCNTs, MWCNTs, SWGONRs, MWGONRs, GONPs, WSNTs, and MSNPs. Raman

spectroscopy analysis (Fig. 2) of SWCNTs, MWCNTs, SWGONRs, MWGONRs, and GONPs showed the characteristic D (1330 – 1340 cm^{-1}), G (1573 – 1586 cm^{-1}), and G' (2650 cm^{-1}) bands of graphene. Structural defects and functional groups are the cause of the first order D band (one phonon double resonance resulting from the disruption of C=C bonds³⁹), the G band is a result of in-plane vibrations involving sp^2 hybridized carbon atoms, and G' band (also called 2D band) is a second order resonance peak of the D band.⁴⁰ Raman peaks at 1330 and 1584 cm^{-1} were observed for SWCNTs [Fig. 2(a)]. The peaks at 1340 and 1573 cm^{-1} were observed for MWCNTs [Fig. 2(b)]. SWGONRs [Fig. 2(c)] showed peaks at 1332 and 1586 cm^{-1} , MWGONRs [Fig. 2(d)] showed peaks at 1336 and 1584 cm^{-1} . GONPs [Fig. 2(e)] showed peaks at 1338 and 1574 cm^{-1} . MSNPs [Fig. 2(f)] showed peaks at 274 and 400 cm^{-1} which can be attributed to E_{1g} vibration modes in the crystalline MoS_2 and its nanohexagonal structure, respectively.¹⁶ The J_2 peak at 230 cm^{-1} showed presence of 2a superlattice while the J_3 peak at 330 cm^{-1} is due to structural distortion. The peaks observed at 816 and 1000 cm^{-1} were due to oxysulfide functional groups.^{17,41} For WSNTs [Fig. 2(g)], the peak at 350 cm^{-1} is due to E_{2g} atomic vibrations for tungsten and sulfur atoms in x-y plane (in opposite direction parallel to x axis), whereas the peak at 420 cm^{-1} corresponded to A_{1g} vibration mode of sulfur atoms in x-y plane (in opposite direction parallel to y axis).^{16,42}

In vitro studies to examine the effects of unreacted macromers

Figures 3(a,b) shows the viability of cells assessed using presto blue assay. This assay exploits the reductive environment of viable cells, and changes the blue-colored resazurin

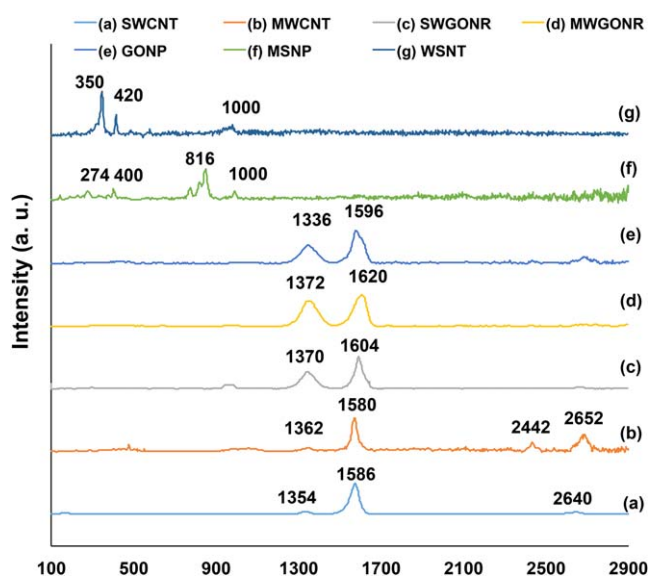


FIGURE 2. Representative Raman spectra of (a) single walled carbon nanotubes, (b) multiwalled carbon nanotubes, (c) single walled graphene oxide nanoribbons, (d) multiwalled graphene oxide nanoribbons, (e) graphene oxide nanoplatelets, (f) molybdenum disulfide nanoplatelets, and (g) tungsten disulfide nanotubes. [Color figure can be viewed in the online issue, which is available at wileyonlinelibrary.com.]

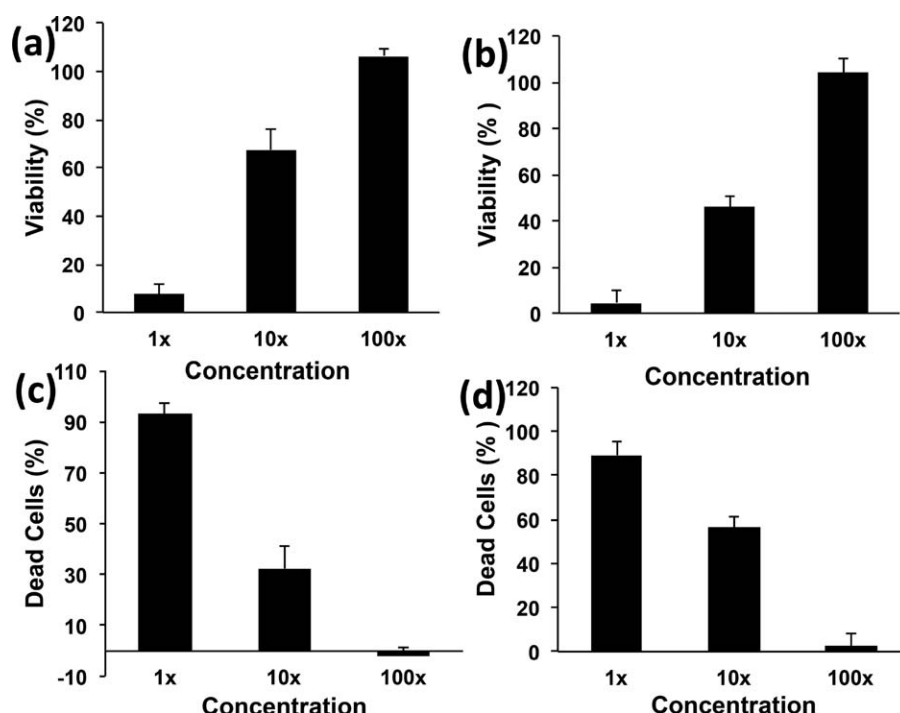


FIGURE 3. Fraction of viable and dead NIH3T3 (a and c) and MC3T3 cells (b and d) after 24 hour exposure to extracts of nanocomposites before crosslinking. Data has been normalized with respect to live and dead controls and error bars represent standard deviations for $n = 6$ samples.

dye into pink-colored resorufin. This alteration indicates cell viability and proliferation.^{43,44} NIH3T3 cells [Fig. 3(a)] showed $8 \pm 3\%$, $63 \pm 9\%$, and $100 \pm 4\%$ viability, after 24 h treatment, using 1X, 10X, and 100X experimental media, respectively. MC3T3 cells [Fig. 3(b)], after 24 h, showed $5 \pm 3\%$, $47 \pm 5\%$, and $105 \pm 4\%$ viability for 1X, 10X, and 100X experimental media, respectively. The experimental media of unreacted components followed a dose dependent viability trend ($1X < 10X$ and $100X$).

The cytotoxicity results obtained from the LDH assay is shown in Figure 3(c,d). LDH, a cytoplasmic marker for membrane integrity, provides an indirect means of assessing cytotoxicity. This assay specifically detects change in light absorbance of assay reagent due to the release of LDH enzyme that catalyzes interconversion of pyruvate (NADH) to lactate (NAD⁺).⁴⁵ NIH3T3 cells [Fig. 3(c)] showed $90 \pm 5\%$, $31 \pm 8\%$, and $2 \pm 5\%$ dead cells for 1X, 10X, and 100X experimental media, respectively. After 24 h, MC3T3 cells [Fig. 3(d)] treated with 1X, 10X, and 100X experimental media showed $89 \pm 10\%$, $55 \pm 4\%$, and $4 \pm 4\%$ dead cells, respectively. The dose dependent cytotoxicity followed the trend: $1X > 10X > 100X$.

In vitro studies to examine the effects of crosslinked nanocomposites

The viability of NIH3T3 and MC3T3 cells analyzed by presto blue assay is reported in Figure 4(a,b). NIH3T3 cells showed greater than 84% viability for all 1X extracts of crosslinked nanocomposites. Cells treated with extracts of MWGONR nanocomposites exhibited $103 \pm 7\%$ viability (maximum), GONP nanocomposites $84 \pm 3\%$ viability (minimum), and PPF control showed $103 \pm 3\%$ viability. Cells treated with 10X and

100X experimental solutions showed $\sim 100\%$ viability for all nanocomposites. MC3T3 cells [Fig. 4(b)] showed more than 78% viability for 1X extracts of crosslinked nanocomposites. Cells treated with MSNP nanocomposites exhibited $89 \pm 2\%$ viability (maximum), MWCNT nanocomposites showed $84 \pm 3\%$ viability (minimum), and PPF control showed $78 \pm 2\%$ viability. Cells treated with 10X and 100X experimental media showed $\sim 100\%$ viability for all nanocomposites. Presto blue results clearly indicated a dose-dependent ($1X < 10$ and $100 X$) viability for crosslinked nanocomposites.

LDH cytotoxicity assay [Fig. 4(c)] for NIH3T3 cells showed $33 \pm 7\%$ cell death (maximum) for MWCNT nanocomposites, $20 \pm 5\%$ cell death (minimum) for WSNT nanocomposites and $25 \pm 8\%$ cell death for PPF control. 10X and 100X experimental media for all nanocomposites showed negligible ($\sim 0\%$) dead cells. MC3T3 cells [Fig. 4(d)] showed $21 \pm 8\%$ (maximum) cell death for MWGONR nanocomposites, $15 \pm 7\%$ dead cells (minimum) for WSNT nanocomposites and $11 \pm 4\%$ dead cells for PPF control. 10X and 100X experimental media of all nanocomposites showed $\sim 0\%$ dead cells. The LDH results of the crosslinked nanocomposites indicated a dose dependent ($1X < 10$ and $100 X$) cytotoxicity.

In vitro studies to examine the effects of degradation products

The results of presto blue and LDH assays are reported in Figure 5. NIH3T3 cells in Figure 5(a) showed more than 23% viability upon treatment with 2X experimental media of degradation products. Cells treated with MSNP nanocomposites showed $48 \pm 3\%$ viability (maximum), GONP nanocomposites showed $23 \pm 4\%$ viability (minimum), and PPF

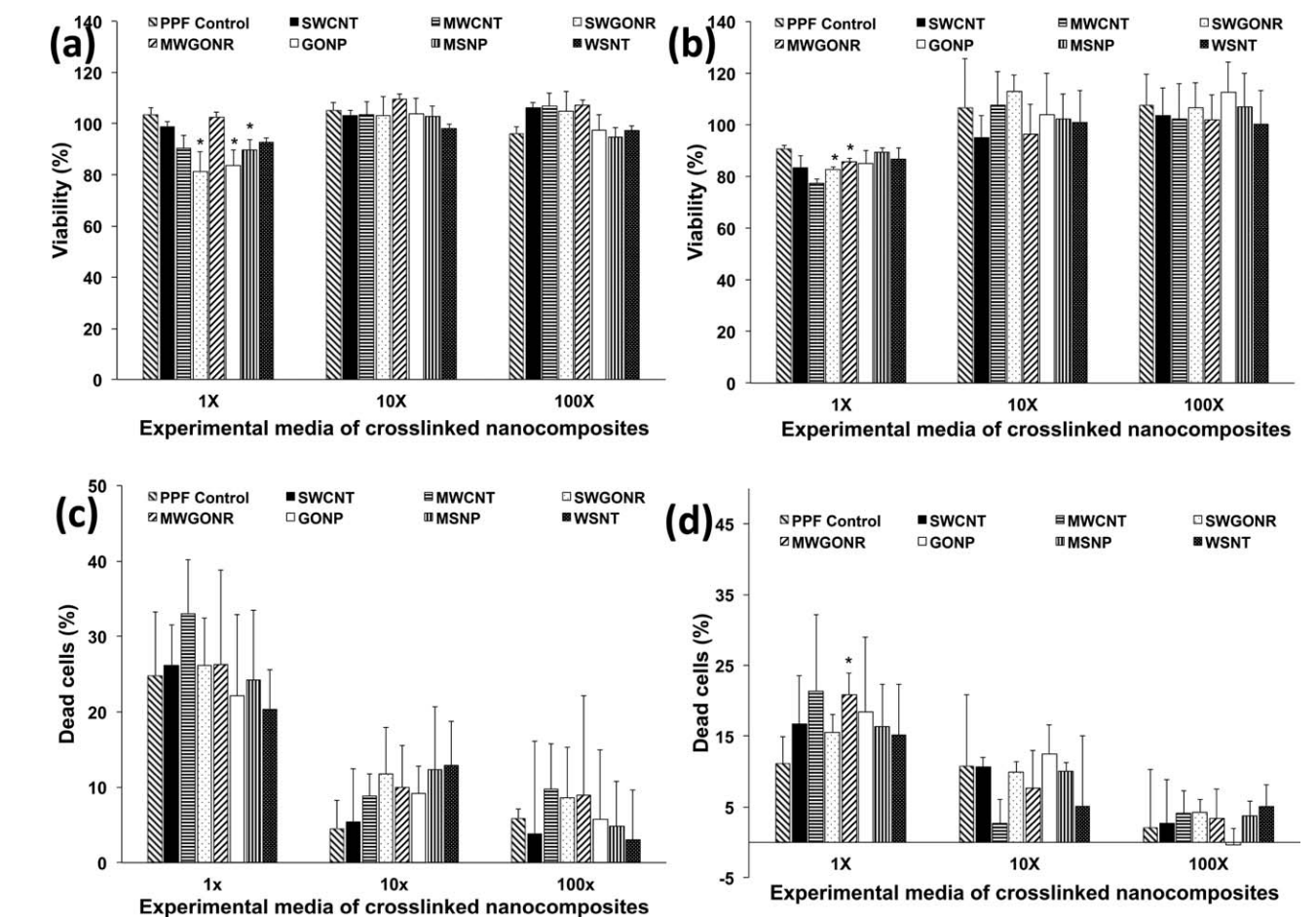


FIGURE 4. Fraction of viable and dead NIH3T3 (a and c) and MC3T3 cells (b and d) after 24 h exposure to extracts of crosslinked nanocomposites. Data has been normalized with respect to live and dead controls and error bars represent standard deviations for $n=6$ samples. The symbol “*” indicates statistical significant difference between PPF baseline and PPF nanocomposites ($p<0.05$).

control showed $38 \pm 2\%$ viability. Cells treated with 10X and 100X experimental media showed 76–97% and 89–104% viability, respectively. In general, MC3T3 cells [Fig. 5(b)] showed more than 25% viability after treatment with 2X experimental media. Cells treated with MSNP nanocomposites exhibited $37 \pm 6\%$ viability (maximum), MWCNT nanocomposites showed $27 \pm 3\%$ viability (minimum), and PPF control showed $37 \pm 5\%$ viability. Cells treated with 10X and 100X experimental media showed $\sim 100\%$ viability.

LDH assay results for NIH3T3 cells treated with 2X experimental media [Fig. 5(c)] showed $65 \pm 8\%$ dead cells (maximum) for MWCNT nanocomposites, $40 \pm 4\%$ dead cells (minimum) for MSNP nanocomposites, and $34 \pm 10\%$ dead cells for PPF control. Cells treated with 10X and 100X experimental media showed 4–23% and 3–8% dead cells, respectively. MC3T3 cells [Fig. 5(d)], indicated $77 \pm 12\%$ dead cells (maximum) for MWCNT nanocomposites, $62 \pm 7\%$ dead cells (minimum) for MSNP nanocomposites, and $67 \pm 10\%$ dead cells for PPF control. Cells treated with 10X and 100X experimental solutions showed 7–20% and 2–17% dead cells, respectively.

Osmolarity (Fig. 6) of all 2X experimental media used for treating NIH3T3 cells were in range of 250–270 mOsm

(significant differences marked with *); significantly lower compared to DMEM media (350 mOsm). Osmolarity of all 2X experimental media used for treating MC3T3 cells were in range of 235–250 mOsm; significantly lower osmolarity compared to MEM- α media (309 mOsm). At 10X and 100X dilutions, osmolarity approached the osmolarity of blank media (350 and 309 mOsm for DMEM and MEM- α , respectively) for both DMEM and MEM- α .

In vitro studies to characterize the cell attachment and spreading on crosslinked nanocomposites

The cell attachment on crosslinked nanocomposites was characterized by counting the number of attached cells using a hemocytometer, after 24 h of incubation. Figure 7 shows the fraction (in percentage) of cells attached to the nanocomposites. The fraction of adherent NIH3T3 cells on nanocomposites [Fig. 7(a)] was between 45 and 57%. The maximum attachment of $57 \pm 1\%$ was observed for WSNT nanocomposites and minimum of $45 \pm 1\%$ for SWCNT nanocomposites. PPF control showed $57 \pm 4\%$ cell attachment whereas TCPS positive control showed $90 \pm 9\%$ cell attachment. Fraction of adherent MC3T3 cells [Fig. 7(b)] on the nanocomposites was between 40–49% of the initial seeded

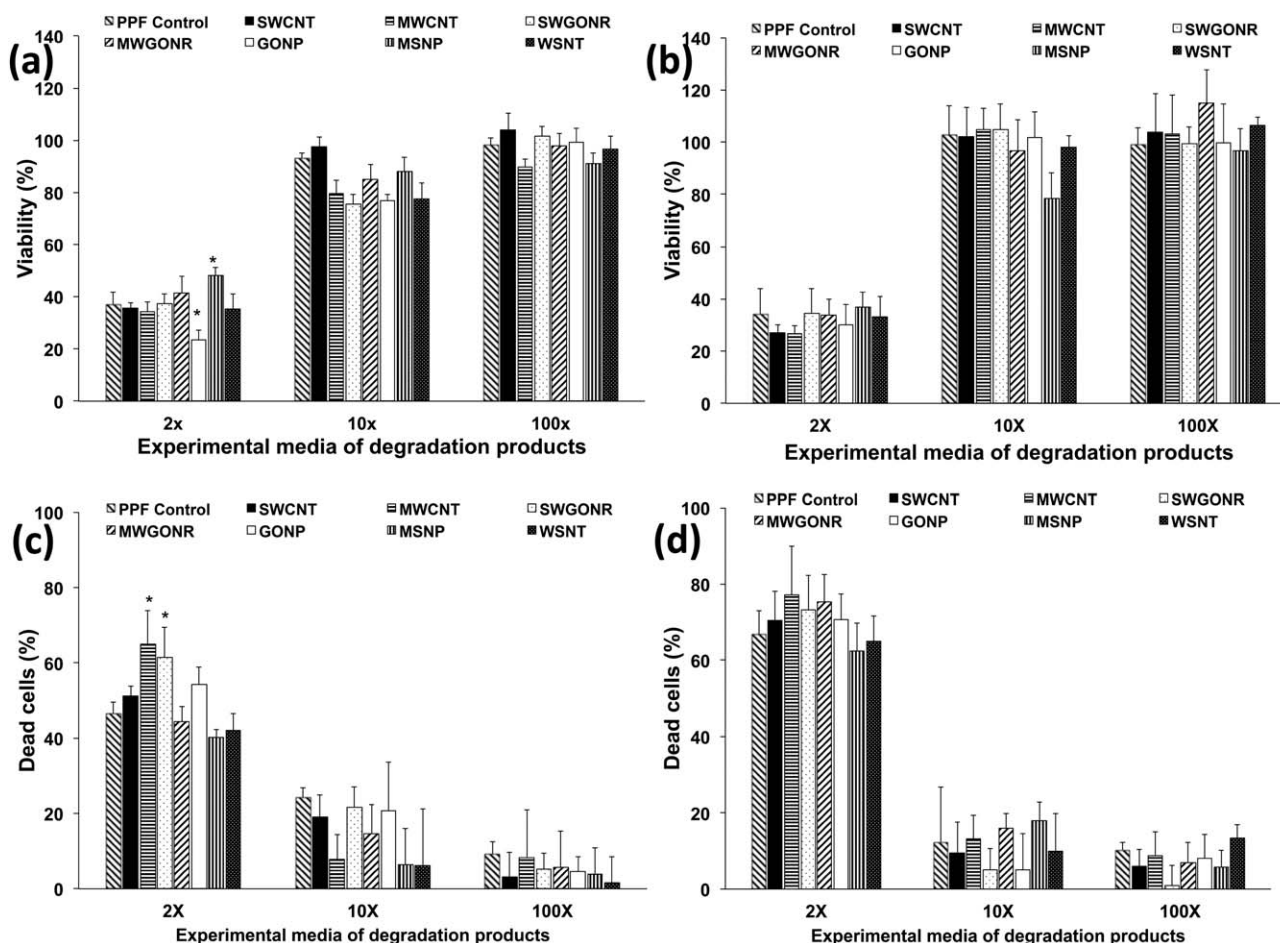


FIGURE 5. Fraction of viable and dead NIH3T3 (a and c) and MC3T3 cells (b and d) after 24 h exposure to extracts of degradation products. Data has been normalized with respect to live and dead controls and error bars represent standard deviations for $n = 6$ samples. The symbol "*" indicates statistical significant difference between PPF baseline and PPF nanocomposites ($p < 0.05$).

cells. WSNT nanocomposites showed maximum attachment of $49 \pm 4\%$ and SWCNT nanocomposites minimum attachment of $40 \pm 2\%$. MC3T3 cell attachment on PPF and TCPS controls was $46 \pm 4\%$ and $93 \pm 3\%$, respectively. Number of attached cells on surface of nanocomposites was significantly lower than TCPS control (marked with ** in Fig. 7). Only SWCNT and MWCNT nanocomposites showed a significantly lower cell attachment compared to PPF control (marked with *). Overall, the presence of nanomaterials evaluated in this study did not have a significant effect on cell attachment compared to PPF control although a greater number of cells attached to inorganic nanocomposites compared to carbon nanocomposites.

Cell attachment and spreading on various nanocomposites was further characterized using confocal fluorescence imaging (Fig. 8) and SEM (Fig. 9). For the fluorescence characterization, calcein-AM dye was used to stain the cells. This dye is a marker for intracellular esterase activity of viable cells indicated by enhanced green fluorescence.⁴⁵ After 5 days of incubation, stained NIH3T3 and MC3T3 cells were observed suggesting viability, attachment and spreading on the nanocomposite surfaces, similar to TCPS control (Fig. 8a). An initial attachment of cells was also observed after 1 day incubation

(Supporting Information Fig. 2S). Circular shape of the cells and incomplete spreading on the surface suggested that additional incubation time was needed to allow the cells to completely spread.

SEM analysis in Figure 9 provided more details regarding cell attachment and spreading on surface of nanocomposites. As seen in Figure 9(a), after 24 h incubation, the surface of nanocomposites was partially covered by round cells [marked with black circles in Fig. 9(a,b)]. Filopodia extensions and extracellular matrix (ECM) formation [white arrows in Fig. 9(b)] were more clearly observed under SEM after incubations for 5 days.

DISCUSSIONS

The objective of this study was to systematically evaluate the *in vitro* cytotoxicity of PPF nanocomposites incorporated with various 1D and 2D carbon (SWCNTs, MWCNTs, SWGONRs, MWGONRs and GONPs) and inorganic (WSNTs and MSNPs) nanomaterials. The loading concentration of each nanomaterial was the concentration that showed maximum reinforcement of PPF polymer in our previous studies.^{16,17} The adherent NIH3T3 fibroblast-like cells^{46,47} and MC3T3 osteoblast precursor cells^{48,49} used in this study are

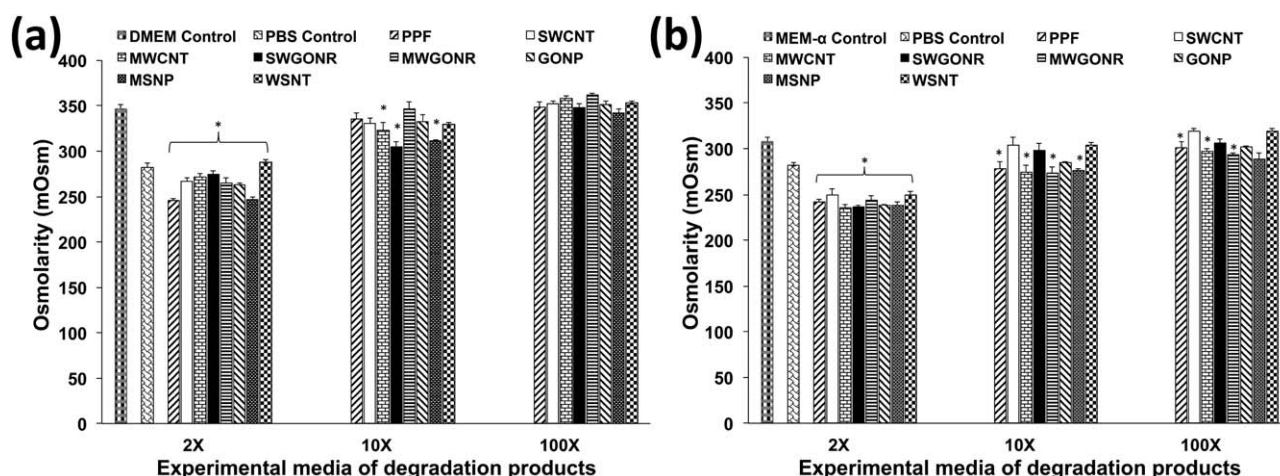


FIGURE 6. Osmolality of extracts of degradation products used for culture for (a) NIH3T3 and (b) MC3T3 cells. Error bars represent standard deviations for $n=3$. The symbol “*” indicates statistical significant difference between extracts of degradation products and unaltered cell culture media ($p < 0.05$).

widely accepted for *in vitro* cytotoxicity testing of materials for orthopedic or bone tissue engineering applications. *In vitro* cytotoxicity studies were performed before crosslinking, after crosslinking, and after accelerated degradation of the nanocomposites. While cytotoxicity of crosslinked nanocomposites and their degradation products is necessary to obtain insights into the possible response of the nanocomposites post *in vivo* implantation,⁵⁰ assessment of cytotoxicity of nanocomposite components before crosslinking is necessary because these components would interact with tissues when injected into bone defect sites.^{26,51}

Presto blue and LDH assays were performed using a cell density of 5000 cells per well. Since LDH is an absorbance-based assay, we used 5000 cells per well to prevent the saturation of the detector of the plate reader and to maintain absorbance values in the linear detectable range. Presto blue and LDH assays are routinely performed using these

cell densities for sensitivity purposes.²³ Previous studies suggest that PPF and PPF nanocomposites show ~50% initial cell attachment (after 24 h) that increases at later time points.²⁹ Therefore, in this study, an initial seeding density of 400,000 cells per specimen was used to ensure good cell attachment for SEM imaging. Fluorescence imaging was performed after days 1 and 5 of initial cell seeding. Considering proliferation of cells, a significantly higher cell number is expected on nanocomposite specimens after 5 days of incubation. Therefore, to ensure good fluorescence staining and to eliminate saturation effects a cell seeding density of 100,000 cells per specimen was used for calcein-AM based fluorescence imaging.

Characterization of polymer and nanomaterials

Structural (TEM) and chemical (Raman spectroscopy) characterizations of the nanomaterials were performed prior to cell

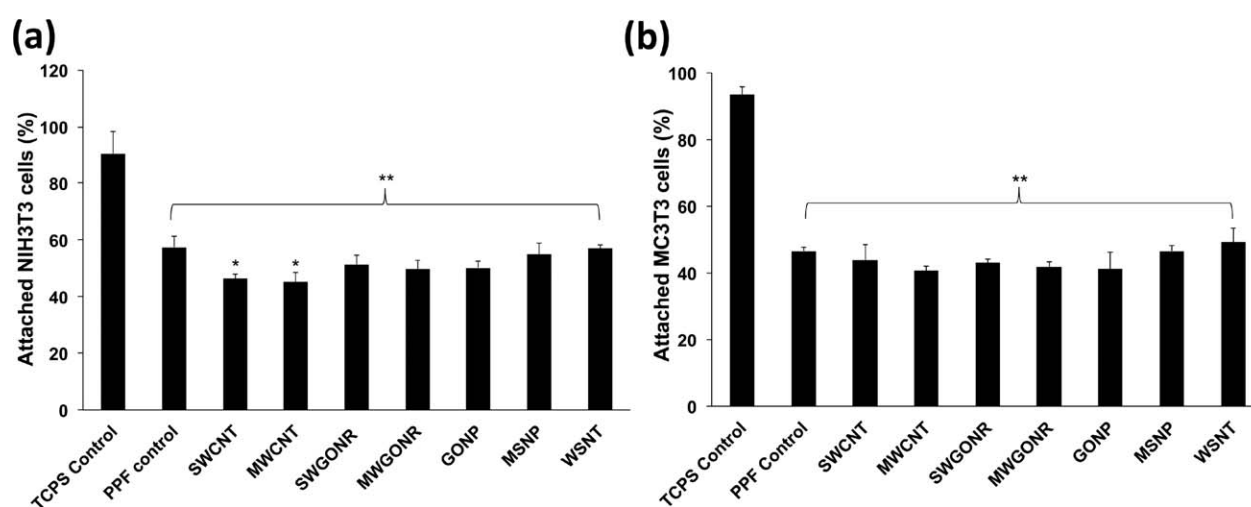


FIGURE 7. Fraction of attached cells to the TCPS, baseline PPF control and nanocomposites after 24 h incubation. Initial seeding density was 400,000 cells/specimen (1.2×10^6 cells/cm²). Error bars represent standard deviations for $n=3$. The symbol “*” indicates statistical significant difference between PPF baseline and PPF nanocomposites. The symbol “**” indicates significant difference between baseline control PPF, PPF nanocomposites and TCPS ($p < 0.05$).

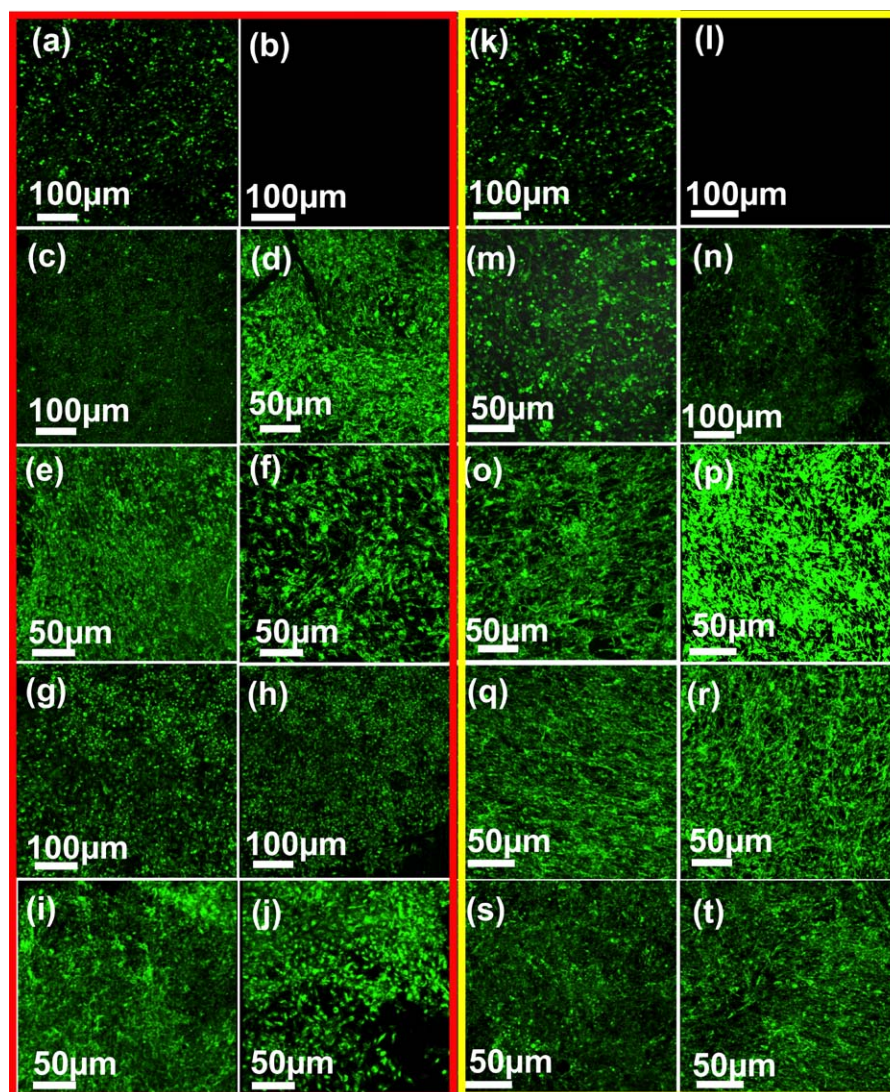


FIGURE 8. Representative fluorescent microscopy images of attached cells on crosslinked nanocomposites after 5 days of cell culture for NIH3T3 (a–j) and MC3T3 (k–t) cells, respectively: (a, k) TCPS (positive control), (b, l) negative control, (c, m) poly(propylene fumarate) control, (d, n) GONP (e, o) MWCNT, (f, p) SWCNT, (g, q) MWGONR, (h, r) SWGONR, (i, s) WSNT, and (j, t) MSNP nanocomposites. [Color figure can be viewed in the online issue, which is available at [wileyonlinelibrary.com](http://www.wileyonlinelibrary.com).]

studies. TEM (Fig. 1) confirmed the tubular morphology of SWCNTs, MWCNTs, and WSNTs; ribbon-shaped morphology of SWGONRs and MWGONRs; disc-shaped morphology of GONPs and hexagonal morphology of MSNPs.^{12,16,23,28,52} Raman spectroscopy analysis (Fig. 2) of SWCNT and MWCNTs showed low intensity ratio of D to G bands (I_D/I_G), which suggests an absence of defects or functional groups on the external carbon sheet. SWGONRs, MWGONRs, and GONPs showed an increase in the intensity ratio of D to G bands (I_D/I_G), which suggests the presence of defects and functional groups that disrupt the sp^2 π -bonds of carbon atoms.^{39,40}

***In vitro* studies to examine the effects of unreacted macromers**

As seen in Figure 3, the cytotoxic effects of unreacted components decreased in a dose-dependent manner after 24 h of incubation. For applications that will employ *in situ* cross-

linking of PPF nanocomposites, the crosslinking reaction time will be a few minutes. In such a scenario, the toxic, leachable components will be minimal. The three components in the uncrosslinked nanocomposites are PPF, nanomaterials and NVP crosslinker. Previous reports show that PPF completely coats the nanomaterials.^{16–18,29} Thus, small PPF oligomers and NVP crosslinker would be the only components that will directly interact with cells in the first 24 h. Therefore, only PPF/ NVP blends were used for preparation of the experimental media. Our results are similar to a previous study that attributed the dose dependent cytotoxicity mainly to the unreacted crosslinker.²⁶

***In vitro* studies to examine the effects of crosslinked nanocomposites**

The high cell viability and low cell death (Fig. 4) observed for 1X, 10X, and 100X experimental media of all the

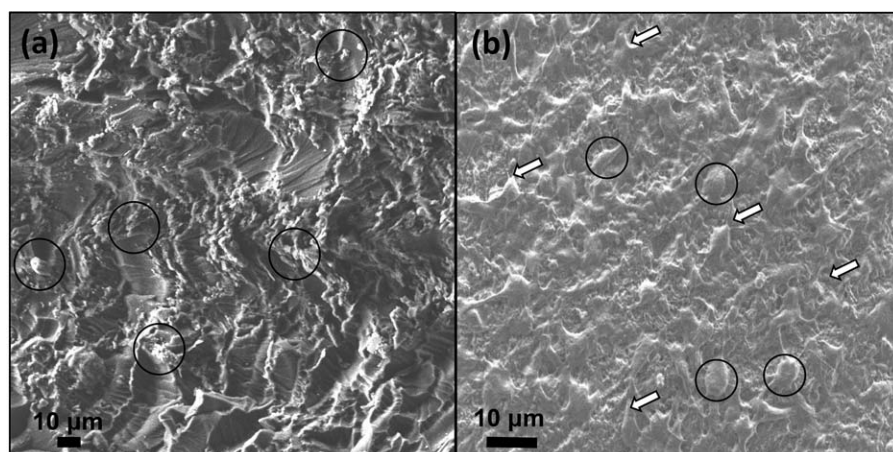


FIGURE 9. Representative SEM images of GONP nanocomposite surface after cell culture for (a) 1 and (b) 5 days (cell bodies are marked with black circles and ECM is marked with white arrows).

crosslinked nanocomposites suggests that improved crosslinking prevented the leaching of potentially toxic components (such as unreacted NVP crosslinker⁵³ and BP radical initiator residue^{54,55}) during media extraction process. Indeed, all but SWGONR crosslinked nanocomposites, had previously exhibited increased crosslinking densities compared to PPF. SWCNT, MWCNT, SWGONR, MWGONR, GONP, MSNP, and WSNT nanocomposites had shown $87 \pm 2\%$, $86 \pm 2\%$, $84 \pm 1\%$, $89 \pm 1\%$, $88 \pm 1\%$, $92 \pm 1\%$, and $92 \pm 2\%$ crosslinking density compared to $84 \pm 2\%$ crosslinking density for PPF polymer, respectively.^{16,17}

***In vitro* studies to examine the effects of degradation products**

The effects of degradation products of nanocomposites on cells during its gradual biodegradation is a necessary factor that needs to be examined for the eventual *in vivo* use of nanocomposites. PPF⁵⁶ and carbon nanomaterials have been reported to undergo biodegradation.⁵⁷ PPF undergoes hydrolytic degradation while carbon nanomaterials can be degraded by oxidative reactions in the presence or absence of enzymes.^{57,58} The degradation of the inorganic nanomaterials still needs to be examined. Crosslinked PPF degrades very slowly, thus an accelerated degradation method is typically employed that hydrolyses the PPF network in 1 week.¹⁸ Earlier reports employed NaOH and HCl to accelerate the hydrolysis of ester bonds in PPF/propylene fumarate-diacrylate (PF-DA). This process caused substantial increase in the osmolality.²⁸ It is well known that high osmolality could be cytotoxic,^{59,60} and thus, it would be difficult to differentiate if any observed toxicity is due to the degraded components or high osmolality. Thus, weaker degrading agents such as calcium hydroxide ($\text{Ca}(\text{OH})_2$) and phosphoric acid (H_3PO_4) that produce insoluble $\text{Ca}_3(\text{PO}_4)_2$ salt crystals after neutralization were used to resolve this issue. Unlike NaCl that undergoes complete ionization and increases osmolality to values higher than 1000 mOsm^{27,59} (compared to plasma osmolality of 282–295 mOsm),

$\text{Ca}_3(\text{PO}_4)_2$ partially ionizes resulting in lower osmolality (235–270 mOsm) of the extracts of degradation products.

In this study, the nanomaterials were present at concentrations of ≤ 0.2 wt %. Thus, given what is known about degradation mechanism of the nanomaterials, and their presence in the polymer matrix at low concentration, the major degradation product that would have an adverse effect on cells would be fumaric acid generated from PPF. The degradation products of PPF, have been previously shown to elicit dose dependent cytotoxicity.^{26,27} Since the dose dependent cell viability and cell death results in Figure 6 are similar to those studies, we hypothesize the degradation products of PPF are mainly responsible for the observed dose dependent cytotoxicity. This low osmolality could also contribute partially to the cytotoxicity results since contact with solutions of lower osmolality brings about damages in cell membrane due to changes in cell volume.

***In vitro* studies to characterize the cell attachment and spreading on crosslinked nanocomposites**

The cell attachment and spreading on the nanocomposites were similar to PPF and lower compared to TCPS control (Fig. 7). The increased cell attachment on TCPS control is due to the negatively charged surface of the TCPS plate that results in better cell spreading and attachment. Variations in the numbers of cells attached to nanocomposites compared to PPF control (Fig. 6) maybe due to different opposing factors that affect cell attachment: nanomaterials (such as MWCNTs⁶¹) result in better adsorption of cell attachment proteins,^{62,63} but presence of attachment inhibitors such as insoluble poly (vinyl pyrrolidone)²⁶ and bundled nanomaterials⁶⁴ hinders cell attachment. In addition to the high density of cells on all nanocomposite surfaces (comparable to PPF control), significant cellular attachment and expansion observed after 5 days [Fig. 8(a,b)] compared to day 1 (Supporting Information Fig. S2) may be the reason for the increased deposition of ECM components on the surface of nanocomposites. As SEM micrograph in Figure 9 showed,

formation of ECM (marked with white arrows) provided a matrix for further cell spreading and proliferation.⁶⁵

To the best of our knowledge, this is the first report that investigates and compares the *in vitro* cytocompatibility of various 1D and 2D carbon and inorganic nanomaterial incorporated polymeric nanocomposites for bone tissue engineering. As mentioned above, the loading concentration of each nanomaterial was one that showed maximum reinforcement of PPF polymer in our previous studies.^{16,17} Thus, even though loading concentrations of all the nanomaterials were low (≤ 0.2 wt %), they were not similar. An initial minor cytotoxicity response and lower cell attachment was observed only for a few nanocomposite groups. None of the nanocomposites showed significant differences in cellular response to the various forms (uncrosslinked, crosslinked and degraded) of nanocomposites compared to PPF control at later time points. The above favorable *in vitro* results suggest that all nanocomposites under these efficacious (enhanced mechanical properties compared to PPF) loading concentrations are suitable for *in vivo* bone replacement therapies.

CONCLUSIONS

Nanocomposites fabricated using biodegradable polymer poly (propylene fumarate), crosslinking agent NVP and 1D and 2D nanomaterials: single- and multi-walled carbon nanotubes, single- and multi-walled graphene oxide nanoribbons, graphene oxide nanoplatelets, molybdenum disulfide nanoplatelets, or tungsten disulfide nanotubes at loading concentrations between 0.02 and 0.2 wt % do not show significant differences in cellular response to their various forms (uncrosslinked, crosslinked and degraded) compared to PPF control. The extraction media of the uncrosslinked components elicit a significant dose-dependent cytotoxic effect. The extraction media of the crosslinked nanocomposite do not adversely affect viability of NIH3T3 and MC3T3 cells. Cells attached, proliferated and spread well on all crosslinked nanocomposite surfaces. The degradation products of nanocomposites induce a mild dose-dependent cytotoxic response. The results demonstrate that all the nanocomposites have favorable *in vitro* cytocompatibility and could be considered further as implants for bone tissue engineering applications.

REFERENCES

- Sabir MI, Xu X, Li L. A review on biodegradable polymeric materials for bone tissue engineering applications. *J Mater Sci* 2009;44: 5713–5724.
- Peter SJ, Miller MJ, Yaszemski MJ, Mikos AG. 5. Polypropylene Fumarate. *Handbook of biodegradable polymers*. Shropshire, United Kingdom: Smithers Rapra; 1998. p 87.
- Santerre J, Woodhouse K, Laroche G, Labow R. Understanding the biodegradation of polyurethanes: From classical implants to tissue engineering materials. *Biomaterials*. 2005;26: 7457–7470.
- Hyon SH, Jin F, Jamshidi K, Tsutsumi S, Kanamoto T. Biodegradable ultra high strength poly (L-lactide) rods for bone fixation. *Macromolecular Symposia: Wiley Online Library*. Weinheim, Germany: WILEY-VCH Verlag GmbH & Co. KGaA; 2003. p 355–368.
- Middleton JC, Tipton AJ. Synthetic biodegradable polymers as orthopedic devices. *Biomaterials*. 2000;21:2335–2346.
- He S, Timmer M, Yaszemski M, Yasko A, Engel P, Mikos A. Synthesis of biodegradable poly (propylene fumarate) networks with poly (propylene fumarate)-diacrylate macromers as crosslinking agents and characterization of their degradation products. *Polymer* 2001;42:1251–1260.
- Suggs LJ, Shive MS, Garcia CA, Anderson JM, Mikos AG. In vitro cytotoxicity and in vivo biocompatibility of poly (propylene fumarate-co-ethylene glycol) hydrogels. *J Biomed Mater Res* 1999;46:22–32.
- Shi X, Mikos AG. Poly (propylene fumarate). Boca Raton, FL: CRC Press; 2006.
- He S, Yaszemski MJ, Yasko AW, Engel PS, Mikos AG. Injectable biodegradable polymer composites based on poly (propylene fumarate) crosslinked with poly (ethylene glycol)-dimethacrylate. *Biomaterials* 2000;21:2389–2394.
- Suggs LJ, West JL, Mikos AG. Platelet adhesion on a bioresorbable poly (propylene fumarate-co-ethylene glycol) copolymer. *Biomaterials* 1999;20:683–90.
- Engh C, Bobyn J, Glassman A. Porous-coated hip replacement. The factors governing bone ingrowth, stress shielding, and clinical results. *J Bone Joint Surg* 1987;69:45–55.
- Lalwani G, Sitharaman B. Multifunctional Fullerene-and Metallofullerene-Based Nanobiomaterials. *Nano LIFE* 2013;3:1342003–1–22.
- Coleman JN, Khan U, Gun'ko YK. Mechanical reinforcement of polymers using carbon nanotubes. *Adv Mater* 2006;18:689–706.
- Mistry AS, Cheng SH, Yeh T, Christenson E, Jansen JA, Mikos AG. Fabrication and in vitro degradation of porous fumarate-based polymer/alumoxane nanocomposite scaffolds for bone tissue engineering. *J Biomed Mater Res Part A*. 2009;89:68–79.
- Balasundaram G, Webster TJ. An overview of nano-polymers for orthopedic applications. *Macromol Biosci*. 2007;7:635–642.
- Lalwani G, Henslee AM, Farshid B, Parmar P, Lin L, Qin Y-X, Mikos AG. Tungsten disulfide nanotubes reinforced biodegradable polymers for bone tissue engineering. *Acta Biomater* 2013;9: 8365–8373.
- Lalwani G, Henslee AM, Farshid B, Lin L, Kasper FK, Qin YX, Mikos AG, Sitharaman B. Two-Dimensional Nanostructure-Reinforced Biodegradable Polymeric Nanocomposites for Bone Tissue Engineering. *Biomacromolecules* 2013;14:900–909.
- Shi X, Sitharaman B, Pham QP, Spicer PP, Hudson JL, Wilson LJ, Liang F, Wu K, Billups E, Mikos AG. In vitro cytotoxicity of single-walled carbon nanotube/biodegradable polymer nanocomposites. *J Biomed Mater Res Part A* 2008;86A:813–823.
- Wang X, Jia G, Wang H, Nie H, Yan L, Deng XY, Wang S. Diameter effects on cytotoxicity of multi-walled carbon nanotubes. *J Nanosci Nanotechnol* 2009;9:3025–3033.
- Akhavan O, Ghaderi E, Akhavan A. Size-dependent genotoxicity of graphene nanoplatelets in human stem cells. *Biomaterials* 2012;33:8017–8025.
- Talukdar Y, Rashkow JT, Lalwani G, Kanakia S, Sitharaman B. The effects of graphene nanostructures on mesenchymal stem cells. *Biomaterials* 2014;35:4863–4877.
- Chang Y, Yang ST, Liu JH, Dong E, Wang Y, Cao A, Yuanfang L, Wang H. In vitro toxicity evaluation of graphene oxide on A549 cells. *Toxicol Lett* 2011;200:201–210.
- Mullick Chowdhury S, Lalwani G, Zhang K, Yang JY, Neville K, Sitharaman B. Cell specific cytotoxicity and uptake of graphene nanoribbons. *Biomaterials* 2013;34:283–293.
- Wu H, Yang R, Song B, Han Q, Li J, Zhang Y, Fang Y, Tenne R, Wang C. Biocompatible inorganic fullerene-like molybdenum disulfide nanoparticles produced by pulsed laser ablation in water. *ACS Nano* 2011;5:1276–1281.
- Pardo M, Shuster-Meiseles T, Levin-Zaidman S, Rudich A, Rudich Y. Low Cytotoxicity of inorganic nanotubes and fullerene-like nanostructures in human bronchial epithelial cells: Relation to inflammatory gene induction and antioxidant response. *Environ Sci Technol* 2014;48:3457–3466.
- Timmer MD, Shin H, Horch RA, Ambrose CG, Mikos AG. In vitro cytotoxicity of injectable and biodegradable poly (propylene fumarate)-based networks: Unreacted macromers, cross-linked networks, and degradation products. *Biomacromolecules* 2003;4: 1026–1033.
- Shi X, Sitharaman B, Pham QP, Spicer PP, Hudson JL, Wilson LJ, Tour JM, Raphael RM, Mikos AG. In vitro cytotoxicity of single-

- walled carbon nanotube/biodegradable polymer nanocomposites. *J Biomed Mater Res Part A* 2008;86:813–823.
28. Sitharaman B, Shi X, Walboomers XF, Liao H, Cuijpers V, Wilson LJ, Mikos AG, Jansen AJ. In vivo biocompatibility of ultra-short single-walled carbon nanotube/biodegradable polymer nanocomposites for bone tissue engineering. *Bone* 2008;43:362–370.
 29. Shi X, Sitharaman B, Pham QP, Liang F, Wu K, Edward Billups W, Wilson LJ, Mikos AG. Fabrication of porous ultra-short single-walled carbon nanotube nanocomposite scaffolds for bone tissue engineering. *Biomaterials* 2007;28:4078–4090.
 30. Mistry AS, Pham QP, Schouten C, Yeh T, Christenson EM, Mikos AG, Jansen JA. In vivo bone biocompatibility and degradation of porous fumarate-based polymer/alumoxane nanocomposites for bone tissue engineering. *J Biomed Mater Res Part A* 2010;92:451–462.
 31. Mistry AS, Mikos AG, Jansen JA. Degradation and biocompatibility of a poly (propylene fumarate)-based/alumoxane nanocomposite for bone tissue engineering. *J Biomed Mater Res Part A* 2007;83:940–953.
 32. Armentano I, Dottori M, Puglia D, Kenny JM. Effects of carbon nanotubes (CNTs) on the processing and in-vitro degradation of poly (DL-lactide-co-glycolide)/CNT films. *J Mater Sci* 2008;19:2377–2387.
 33. Yoon OJ, Jung CY, Sohn IY, Kim HJ, Hong B, Jhon MS, Lee NE. Nanocomposite nanofibers of poly (d, l-lactic-co-glycolic acid) and graphene oxide nanosheets. *Compos Part A: Appl Sci Manuf* 2011;42:1978–1984.
 34. Jing X, Mi HY, Salick MR, Peng XF, Turng LS. Preparation of thermoplastic polyurethane/graphene oxide composite scaffolds by thermally induced phase separation. *Polym Compos*. Forthcoming.
 35. Kasper FK, Tanahashi K, Fisher JP, Mikos AG. Synthesis of poly (propylene fumarate). *Nat Protoc* 2009;4:518–525.
 36. Kosynkin DV, Higginbotham AL, Sinitskii A, Lomeda JR, Dimiev A, Price BK, Tour JM. Longitudinal unzipping of carbon nanotubes to form graphene nanoribbons. *Nature* 2009;458:872–876.
 37. Lalwani G, Sundararaj JL, Schaefer K, Button T, Sitharaman B. Synthesis, characterization, in vitro phantom imaging, and cytotoxicity of a novel graphene-based multimodal magnetic resonance imaging-X-ray computed tomography contrast agent. *J Mater Chem B* 2014;2:3519–3530.
 38. Castro-Guerrero CF, Deepak FL, Ponce A, Cruz-Reyes J, Del Valle-Granados M, Fuentes-Moyado S, Galvan DH, Jose-Yacamán M. Structure and catalytic properties of hexagonal molybdenum disulfide nanoplates. *Catal Sci Technol* 2011;1:1024–1031.
 39. Malard L, Pimenta M, Dresselhaus G, Dresselhaus M. Raman spectroscopy in graphene. *Phys Rep* 2009;473:51–87.
 40. Iqbal M, Singh AK, Iqbal M, Eom J. Raman fingerprint of doping due to metal adsorbates on graphene. *J Phys: Condens Matter* 2012;24:335301.
 41. Bar-Sadan M, Enyashin A, Gemming S, Popovitz-Biro R, Hong S, Prior Y, Tenne R, Seifert G. Structure and stability of molybdenum sulfide fullerenes. *J Phys Chem B* 2006;110:25399–25410.
 42. Rothschild A, Frey G, Homyonfer M, Tenne R, Rappaport M. Synthesis of bulk WS₂ nanotube phases. *Mater Res Innov* 1999;3:145–149.
 43. Butterick TA, Nixon JP, Pérez-Leighton CE, Billington CJ, Kotz CM. Orexin A influences lipid peroxidation and neuronal metabolic status in a novel immortalized hypothalamic cell line. Washington, DC: Society for Neuroscience. Abstracts 2011, 2011. p 88.
 44. Bueno C, Villegas ML, Bertolotti SG, Previtali CM, Neumann MG, Encinas MV. The excited-state interaction of resazurin and resorufin with amines in aqueous solutions. *Photophys Photochem React* 2002;76:385–390.
 45. Decker T, Lohmann-Matthes M-L. A quick and simple method for the quantitation of lactate dehydrogenase release in measurements of cellular cytotoxicity and tumor necrosis factor (TNF) activity. *J Immunol Methods* 1988;115:61–69.
 46. Lee Y, Geckeler KE. Cytotoxicity and cellular uptake of lysozyme-stabilized gold nanoparticles. *J Biomed Mater Res Part A* 2012;100:848–855.
 47. Zhao H, Zhu B, Sekine J, Luo S-C, Yu H-h. Oligoethylene-glycol-functionalized polyoxythiophenes for cell engineering: Syntheses, characterizations, and cell compatibilities. *ACS Appl Mater Interfaces* 2012;4:680–686.
 48. Wang K, Cai L, Jesse S, Wang S. Poly (ε-caprolactone)-Banded Spherulites and Interaction with MC3T3-E1 Cells. *Langmuir* 2012;28:4382–4395.
 49. Sahoo NG, Pan YZ, Li L, He CB. Nanocomposites for bone tissue regeneration. *Nanomedicine* 2013;8:639–653.
 50. Liu H, Webster TJ. Nanomedicine for implants: A review of studies and necessary experimental tools. *Biomaterials* 2007;28:354–369.
 51. Sitharaman B, Shi X, Tran LA, Spicer PP, Rusakova I, Wilson LJ, Mikos AG. Injectable in situ cross-linkable nanocomposites of biodegradable polymers and carbon nanostructures for bone tissue engineering. *J Biomater Sci* 2007;18:655–671.
 52. Lalwani G, Kwaczala AT, Kanakia S, Patel SC, Judex S, Sitharaman B. Fabrication and characterization of three-dimensional macroscopic all-carbon scaffolds. *Carbon* 2013;53:90–100.
 53. Timmer MD, Ambrose CG, Mikos AG. In vitro degradation of polymeric networks of poly (propylene fumarate) and the cross-linking macromer poly (propylene fumarate)-diacrylate. *Biomaterials* 2003;24:571–577.
 54. Swauger JE, Dolan PM, Zweier JL, Kuppusamy P, Kensler TW. Role of the benzoyloxyl radical in DNA damage mediated by benzoyl peroxide. *Chem Res Toxicol* 1991;4:223–228.
 55. Cameron G, Bryce W, McWalter I. Thermal degradation of polystyrene—5. Effects of initiator residues. *Eur Polym J* 1984;20:563–569.
 56. Timmer MD, Ambrose CG, Mikos AG. Evaluation of thermal-and photo-crosslinked biodegradable poly (propylene fumarate)-based networks. *J Biomed Mater Res Part A* 2003;66:811–818.
 57. Kotchey GP, Hasan SA, Kapralov AA, Ha SH, Kim K, Shvedova AA, Kagan VE, Star A. A Natural Vanishing Act: The enzyme-catalyzed degradation of carbon nanomaterials. *Acc Chem Res* 2012;45:1770–1781.
 58. Xing W, Lalwani G, Rusakova I, Sitharaman B. Degradation of Graphene by Hydrogen Peroxide. *Particle Particle Syst Charact* 2014;31:745–750.
 59. Waymouth C. Osmolality of mammalian blood and of media for culture of mammalian cells. *In Vitro* 1970;6:109–127.
 60. Higgins CB, Sovak M, Schmidt WS, Kelley MJ, Newell JD. Direct myocardial effects of intracoronary administration of new contrast materials with low osmolality. *Invest Radiol* 1980;15:39–46.
 61. Ge C, Du J, Zhao L, Wang L, Liu Y, Li D, Zhoro Y, Zhifang C, Chunying C. Binding of blood proteins to carbon nanotubes reduces cytotoxicity. *Proc Natl Acad Sci USA* 2011;108:16968–16973.
 62. Khang D, Kim SY, Liu-Snyder P, Palmore GTR, Durbin SM, Webster TJ. Enhanced fibronectin adsorption on carbon nanotube/poly (carbonate) urethane: Independent role of surface nano-roughness and associated surface energy. *Biomaterials* 2007;28:4756–4768.
 63. Kane RS, Stroock AD. Nanobiotechnology: Protein-nanomaterial interactions. *Biotechnol Prog* 2007;23:316–319.
 64. Cui D, Tian F, Ozkan CS, Wang M, Gao H. Effect of single wall carbon nanotubes on human HEK293 cells. *Toxicol Lett* 2005;155:73–85.
 65. Bryant SJ, Anseth KS. Controlling the spatial distribution of ECM components in degradable PEG hydrogels for tissue engineering cartilage. *J Biomed Mater Res Part A* 2003;64:70–79.